MATERIALS CHEMISTRY
FRONTIERS
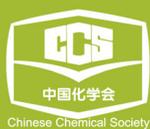
RESEARCH ARTICLE

Iron nanoparticles-based supramolecular hydrogels to originate anisotropic hybrid materials with enhanced mechanical strength†

Rafael Contreras-Montoya,[a] Ana B. Bonhome-Espinosa,[b] Angel Orte, [ID][c] Delia Miguel, [ID][c] Jose M. Delgado-López, [ID]‡[d] Juan D. G. Duran, [ID][b] Juan M. Cuerva, [ID][a] Modesto T. Lopez-Lopez [ID]*[b] and Luis Álvarez de Cienfuegos [ID]*[a]

Here, we report the synthesis and structural characterization of novel iron nanoparticles (FeNPs)-based short-peptide supramolecular hydrogels. These hybrid hydrogels composed of Fmoc-diphenylalanine (Fmoc-FF) peptide and FeNPs were prepared through the self-assembly of Fmoc-FF in a suspension containing FeNPs in the presence or absence of an external magnetic field. Optical images of these hydrogels revealed the formation of column-like aggregates of FeNPs when the gels were formed in the presence of a magnetic field. Moreover, the intricate structure derived from the interwoven nature of the fiber peptides with these FeNP column-like aggregates resulted in anisotropic materials, more rigid under shear forces applied perpendicularly to the direction of the aggregates, presenting under these conditions values of G′ (storage modulus) about 7 times those of the native hydrogel. To the best of our knowledge, this is the first example in which the mechanical properties of peptide hydrogels were strongly enhanced due to the presence of FeNPs. A theoretical model trying to explain this phenomenon is presented. Quite interesting CD, FTIR and synchrotron X-ray diffraction analyses indicated that the anti-parallel β-sheet arrangement of Fmoc-FF peptide was highly conserved in the hydrogels containing FeNPs. Moreover, FLCS measurements showed that the diffusion of a small solute through the hydrogel network was improved in hydrogels containing FeNPs, probably caused by the formation of preferential channels for diffusion. Taken together, our results provide a new method for the synthesis of novel hybrid Fmoc-FF–FeNPs anisotropic hydrogels with enhanced mechanical strength and water-like diffusion behavior, thus easing their application in drug delivery and tissue engineering.

[a] Dpto de Química Orgánica, Facultad de Ciencias, Universidad de Granada (UGR), 18071-Granada, Spain. E-mail: lac@ugr.es

[b] Dpto de Física Aplicada, Facultad de Ciencias, (UGR), 18071-Granada, Spain. E-mail: modesto@ugr.es

[c] Dpto de FisicoQuímica, Facultad de Farmacia, (UGR), 18072-Granada, Spain

[d] Laboratorio de Estudios Cristalográficos, Instituto Andaluz de Ciencias de la Tierra (Consejo Superior de Investigaciones Científicas-Universidad de Granada), Avenida de las Palmeras 4, 18100 Armilla, Granada, Spain

† Electronic supplementary information (ESI) available: Supplementary figures. See DOI: 10.1039/c7qm00573c

‡ Present address: Dpto de Química Inorgánica, Facultad de Ciencias, (UGR), Spain.

Introduction

Hydrogels are an important class of materials that have found useful technological and biotechnological applications due to their high water content and diverse mechanical properties. Moreover, these types of materials can be chemically designed to respond to different external stimuli with the intention of provoking in the hydrogel a physical or chemical change (*i.e.*, altering their mechanical properties or triggering the release of substances, *etc.*), making them what have been termed "smart materials".[1] An important category of these stimuli-sensitive hydrogels are magnetic hydrogels or ferrogels (*i.e.*, the combination of hydrogels with micro- and/or nano-magnetic particles (MPs)) (*e.g.*, γ-Fe$_2$O$_3$, Fe$_3$O$_4$, CoFe$_2$O$_4$) that are able to respond to an external magnetic field, modifying their properties (from the microstructure shape and size to the mechanical behavior).[2] The possibility of altering their properties remotely makes them very appealing for multiple applications, such as pulsatile delivery vehicles, magnetic resonance imaging contrast agents, hyperthermal therapy agents, *etc.* The properties of these composite materials rely on several factors, such as the nature of the hydrogel, the type of interaction (physical or chemical) between the fibers and MPs, and the concentration, size and distribution of the MPs within the hydrogels. Additionally, the method of preparation can also

have an influence on the final properties of the ferrogel.[3] Nevertheless, the interesting properties of these materials have been mainly restricted to polymers due to their great versatility and capacity to modify their structure.

Recently, supramolecular hydrogels composed of small molecules (low molecular weight gelators, LMWG) able to self-assemble by an external stimulus have turned into excellent candidates for the construction of smart and functional materials.[4] The dynamic nature of the non-covalent self-association makes them more prone to be modified by external stimuli, which in most cases promote a change in the macroscopic properties of these materials causing them to evolve into systems that are adaptive to the environment.[5] Short-peptide supramolecular hydrogels are an example of this kind of materials.[6] These peptides have a strong tendency to self-associate requiring in most of the cases less than 1 wt% to immobilize the aqueous medium. Due to their chemical structure, these compounds are able to form gels by different stimuli or conditions, mainly solvent, pH and/or temperature changes or enzymatic reaction.[6a,7] The stimulus triggers the self-association process and, as a consequence, different stimuli can differently affect the structural and mechanical properties of the resulting gel. In this sense, much effort has been focused on modifying the mechanical properties of these hydrogels since many useful applications depend on the rheological performance of these materials.[8] For example, it is known that dipeptide LMWG derivative gels can be formed by pH and solvent switch and using one or the other stimulus has an effect on the mechanical properties of the gels, even the homogenization techniques and the final solvent content also have an impact.[9] Alternatively, one strategy to modulate the mechanical properties of these hydrogels has been the development of composite materials by the combination of these peptides with others or with different additives. In this sense, the mechanical properties of hybrid hydrogels composed of Fmoc-FF and Fmoc-K, Fmoc-D or Fmoc-S have shown lower elastic moduli[10a] or higher mechanical strength (Fmoc-RGD)[10b] compared to Fmoc-FF alone. The presence of polymers such as dextrans,[11] agarose,[12] and konjac glucomannan[13] has shown mixed results, causing, in some cases, a decrease in the mechanical properties of the gel (dextrans); an increase in the fracture stress (agarose); and an increase in the stability and mechanical strength (konjac glucomannan). Furthermore, the incorporation of solid nanoparticles, such as AgNPs,[14] carbon nanotubes (CNTs),[15] and graphene,[16] has also decreased (AgNPs) or increased (CNTs and graphene) the mechanical strength of the hydrogels. Interestingly, the incorporation of solid nanoparticles in the gel matrix can also provide new properties to these materials, such as antibacterial and/or fluorescence properties (AgNPs), and electrical conductivity (CNTs). Additionally, certain nanoparticles are able to exert a structural control over the distribution of the supramolecular nanofibers.[17]

Based on these precedents, herein, we report the synthesis and characterization of novel magnetic supramolecular hydrogels composed by the self-association of Fmoc-FF in the presence of different ratios of core–shell Fe nanoparticles with a polyethylene glycol covering (Fe nanoparticles@PEG) under the influence or absence of an external magnetic field. Our results indicate that
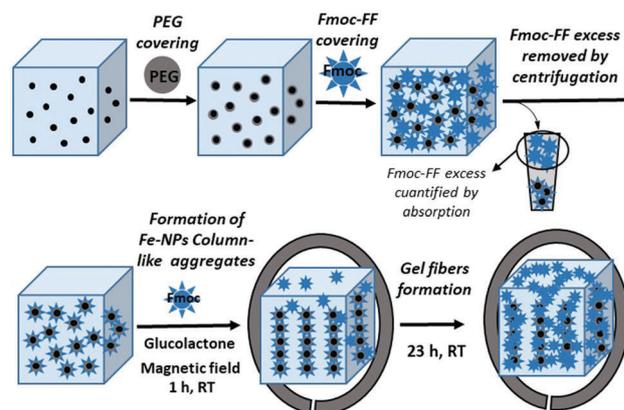

Fig. 1 Sketch of the preparation protocol of magnetic hydrogels.

when they were prepared under an applied magnetic field, the mechanical properties (measured under shear applied perpendicular to the field direction) of these magnetic hydrogels improve dramatically, up to 7 times, with respect to the nonmagnetic or randomly oriented magnetic nanoparticles hydrogels, whilst, at the same time, the diffusion of a solute through the structure is improved. This improvement in their mechanical properties occurs only when the gel is formed in the presence of an applied magnetic field and is the consequence of a particular combination of structural characteristics in the hydrogel. These structural characteristics imply the engulfment of magnetically oriented FeNP column-like structures by the peptide fibers that have been formed in the presence of them (see Fig. 1). We have checked that this anisotropy at the microscopic level is also reflected in the macroscopic mechanical properties of the magnetic hydrogels, which present weaker rheological moduli when the applied shear is within the same plane of the FeNP column-like structures.

Quite interestingly, the non-covalent nature of this self-association allows the inclusion of these FeNP column-like structures within the peptide network to give a homogeneous hybrid material without practically modifying the secondary structure of the peptide. Surprisingly, this 700% improvement of the mechanical properties of the magnetic hydrogels takes place with a tiny (0.6 vol%) amount of FeNPs. The simple embedment of the FeNPs within the matrix of the hydrogel cannot justify such a large enhancement; in fact, the classical theory of mechanics of composite materials[18] only predicts an enhancement of the mechanical properties of the order of 1% when such an amount of spherical particles is embedded within a continuous matrix. We demonstrate in our work that the application of a magnetic field to the pre-gel mixture induces the aggregation of FeNPs into column-like structures. The particles within the structures are subsequently engulfed by the gel-forming peptides, in such a way that these structures are maintained even after magnetic field removal, serving as scaffolding for the support and mechanical enhancement of the resulting hydrogels, something that to the best of our knowledge has not been previously reported for biological gels. Moreover, these magnetic hydrogels, similar to the Fmoc-FF

hydrogel, can be extruded through a syringe keeping their gel state.[19] All of these new properties, together with the known biocompatibility and biodegradability of these hydrogels, provide these materials with useful potential applications in several biomedical fields, such as drug delivery agents and tissue engineering. To gain in-depth insights into the morphological and structural properties of these materials, these hydrogels have been studied by magnetization, optical microscopy, environmental scanning electron microscopy, infrared spectroscopy, circular dichroism, X-ray diffraction and synchrotron X-ray total scattering, fluorescence lifetime correlation spectroscopy and rheology. It is worth noting that a magnetic supramolecular hydrogel in which the gel to sol transition is triggered by an external magnetic field has been successfully prepared although a study of its mechanical properties has not been reported.[20]

Experimental

Reagents and materials

N-Fluorenylmethoxycarbonyl diphenylalanine (Fmoc-FF) was purchased from Bachem Co., Switzerland and was used without further purification. Fe nanopowders/nanoparticles, 99.7+%, 60–80 nm, were purchased from SkySpring Nanomaterials, Inc., Houston, USA. PEG-400 (polyethylene glycol, 400 g mol^{-1}), glutaraldehyde (25% solution in water), mineral oil and sorbitan sesquioleate were provided by Sigma-Aldrich, USA. *n*-Hexane, min 99%, was purchased from Scharlab S.L., Spain. D(+)-Glucono-1,5-lactone 99% was purchased from Alfa Aesar, Germany. Sodium nitrate (for analysis) was purchased from Merck, Germany.

Preparation of magnetic nanoparticles with PEG coating

As the magnetic phase, we used iron nanopowders consisting of iron nanoparticles (FeNPs) of diameter in the range 60–80 nm. In order to avoid corrosion, the manufacturer provides the particles in vacuum bags, which we opened under an argon atmosphere to reduce contact with oxygen. Immediately afterwards, the nanoparticles were coated with a layer of polyethylene glycol (PEG), which protects from corrosion, as we proved in a previous work.[21] Furthermore, the PEG coating also imparts to the particles the biocompatibility required for biomedical applications. Indeed, coating nanoparticles with a PEG layer reduces the attack by macrophages, as has been shown.[22] For the PEG coating, we adapted the water-in-oil emulsion method described by Chatterjee *et al.*[23] Briefly, we prepared a water phase that consisted of a mixture of 200 mg of FeNPs and 1 g of PEG-400 in purified water (Milli-Q quality, Millipore Corporation), previously purged with argon in order to remove oxygen and prevent the iron NPs from corrosion. This mixture was homogenized by an ultrasonic bath for 7 minutes. Separately, we prepared the oil phase consisting of 450 mL of hexane, 150 mL of mineral oil and 0.75 mL of sorbitan sesquioleate. Afterwards, we mixed both (water and oil) phases and sonicated them for 5 minutes in order to obtain a water-in-oil microemulsion. Subsequently, we added 150 mL of glutaraldehyde under mechanical stirring – note that glutaraldehyde is responsible for the initiation of the polymerization

of PEG. The reaction was maintained for 2 hours under mechanical stirring. Finally, the magnetic product was separated by magnetic decantation and repeatedly washed with ethanol and purified water (Milli-Q quality). Pristine iron nanoparticles will be referred to as PMNP (Pristine Magnetic NanoParticles), while PEG-coated iron nanoparticles are called MNP@PEG.

Characterization of the nanoparticles

The size and shape of PMNP and MNP@PEG were characterized by transmission electron microscopy (TEM). The effectiveness of the PEG coating was confirmed by measuring the electrophoretic mobility at different pH values using a Nano Zs, Zetasizer Instrument (Malvern). For this method, both PMNP and MNP@PEG were suspended in 1 mM solutions of NaNO$_3$. Then, for each of the powders (pristine and coated), in order to determine their isoelectric point, we adjusted the pH of the suspensions of iron nanoparticles in NaNO$_3$ within precise values within the range 4–11, using 0.1 M solutions of NaOH or HNO$_3$. Measurements, in triplicate for each sample, were carried out at 25 °C using disposable plastic cuvettes.

Finally, we characterized the magnetic properties of the dry nanopowders by using a Quamtum Design NPMS X magnetometer.

Nonmagnetic hydrogel (NMHG) preparation

The NMHG gelification was performed following a previously reported described protocol.[24] Very briefly, Fmoc-FF peptide was weighed into a sample tube and deionised water was added to obtain a final concentration of 0.5% (w/v). This suspension was then sonicated (in a HSt Powersonic 603-ultrasonic bath) for 10 minutes. Little portions of 0.5 M NaOH solution, were then added by pipette. The solution was vortexed (using an LBX V05 series vortex stirrer) and sonicated after each addition to aid mixing, until a clear solution was obtained at a pH of approximately 10.35. (The pH was measured using a HACH sension™ PH 3 pH meter. The pH meter was calibrated using pH 4, pH 7 and pH 10 buffer solutions.) This solution was diluted with deionised water (or 2.5 nM fluorescence dye solution for FLCS studies) to obtain a final Fmoc-FF concentration of 0.3% (w/v). Gelation was then carried out by addition of 2 molar equivalents of glucono-δ-lactone (GdL) to the basic peptide solution and mixing was achieved by vortexing for 5 seconds. According to rheological measurements, full gelification at room temperature was achieved after 12 h.

MNP@PEG@Fmoc-FF nanoparticles preparation

100 mg of MNP@PEG was suspended in 1.5 mL of an aqueous basic solution of Fmoc-FF 0.5% (w/v). The resulting suspension was sonicated for 10 min and then centrifuged for 5 min at 10 000 rpm (Sigma 1-14 centrifuge); afterwards, the supernatant was removed (see sketch in Fig. 1). The quantification of the amount of Fmoc-FF adsorbed on MNP@PEG was calculated by absorption measurements. For this purpose, the absorbance of Fmoc-FF solutions of different concentrations was measured at the maximum of absorption (266 nm), obtaining a good linear relationship between absorbance and concentration. Then, the remaining amount of Fmoc-FF in the supernatant was measured

688 | *Mater. Chem. Front.*, 2018, **2**, 686–699

This journal is © The Royal Society of Chemistry and the Chinese Chemical Society 2018

spectrophotometrically using an Analytik Jena SPECORD® 200 Plus and thus concentration was obtained from the interpolation in the previous fitting (see Fig. S1 of the ESI†). From the average of three measurements, it was found that the adsorption of Fmoc-FF on MNP@PEG was 4.7775×10^{-2} g Fmoc-FF per gram of MNP@PEG. To further confirm the Fmoc-FF adsorption on MNP@PEG, we performed measurements of the electrophoretic mobility of the new MNP@PEG@Fmoc-FF particles following a similar protocol to the described for the PEG-coated MNP.

MNP@PEG@Fmoc-FF composite hydrogel preparation

To an aqueous basic solution of Fmoc-FF 0.5% (w/v), the suitable weighted amount of MNP@PEG@Fmoc-FF particles to obtain the different final concentrations of 0.05 vol%, 0.1 vol%, 0.3 vol%, 0.6 vol%, and 0.9 vol%, corresponding to hydrogels MHG-0.05, MHG-0.1, MHG-0.3, MHG-0.6 and MHG-0.9, was added and diluted to a final Fmoc-FF concentration of 0.3% (w/v). This suspension was sonicated for 5 min to give a homogeneous suspension. This suspension was gelified by the addition of GdL, keeping it at room temperature for 24 h. To obtain the hydrogels with FeNPs aligned into column-like structures, after the addition of GdL and for 1 hour, the hydrogel was kept under the influence of a vertically applied magnetic field of 15 kA m^{-1} strength (we used a solenoid connected to a DC power supply for this purpose), followed by 23 h without the stimulus of the magnetic field at room temperature (Fig. 1).

Characterization of the magnetic properties of the hydrogels

We obtained the magnetization curve of the magnetic hydrogels by means of a Quamtum Design NPMS X magnetometer. For this method, we applied different values of the magnetic field and measured the resulting magnetization of the samples.

Optical microscopy

We analyzed the mesoscopic structure of the hydrogels by direct observation with an optical microscope (Nikon, SMZ800) at $5\times$ magnification. We took photos of hydrogels prepared by different experimental protocols using a CCD camera (Pixelink, Canada) connected to the microscope.

Electron microscopy

TEM images of FeNPs. The nanoparticles used in this work were studied with a LIBRA 120 PLUS Carl Zeiss. A drop of an ethanolic suspension of PMNP and MNP@PEG was placed on a 300-mesh copper grid. The sample was dried at room temperature for 30 min.

ESEM images of hydrogels. Hydrogel images were obtained using an FEI Quanta 400 ESEM equipped with a Peltier effect cooling stage.

Circular dichroism (CD)

The CD spectra were recorded using an Olis DSM172 spectro-fotometer with a xenon lamp of 150 W. The hydrogels were gelified into a 0.1 mm quartz cell (Hellma 0.1 mm quartz Suprasil®) using the protocol described above. Spectra were obtained from 200 to 320 nm with a 1 nm step and 0.1 s integration

time per step at 25 °C. The data shown correspond to the average of 20 measurements.

Fourier transform infra-red (FTIR) spectroscopy

Spectra were recorded using a Perkin-Elmer Two FTIR ATR spectrometer. The hydrogels and the xerogel were compressed onto the diamond crystal. All spectra were scanned over the range between 4000 and 450 cm^{-1}.

X-ray diffraction (XRD)

X-ray diffraction patterns were obtained with Cu Kα radiation (λ = 1.5418 Å) on a PANalytical X'Pert PRO diffractometer equipped with a PIXcel detector operating at 45 kV and 40 mA. The 2θ range was from 5° to 80° with a step size of (2θ) 0.039°. By varying the scattering angle, the explored momentum transfer vector (q) was in the range of $1 < q$ (nm^{-1}) < 28.0, with $q = (4p/k)\sin h$, where h is the scattering angle. A freshly prepared gel was deposited on a silicon holder and dried overnight prior to data collection.

Synchrotron X-ray total scattering

Dried gels were loaded in glass capillaries of 0.8 mm diameter and measured at the X04SA-MS Beamline of the Swiss Light Source (SLS) of the Paul Scherrer Institut (PSI, Villigen, CH). The beam energy was set at 16 keV and the operational wavelength (λ = 0.77627 Å) precisely determined by collecting, under the same experimental conditions, a silicon powder standard [NIST 640c, a_0 = 0.54311946(92) nm at 22.5 °C]. A position sensitive single-photon counting MYTHEN II was used as a detector. Independent He/air and capillary scattering curves, as well as empty and sample-loaded capillary transmission coefficients, were also measured and used for data subtraction of all extra-sample scattering effects and absorption correction.

Fluorescence lifetime correlation spectroscopy

Fluorescence fluctuation traces of a xanthene derivative dye, 4-methoxy-Pennsylvania Green (**4-OMe-PG**),[25] dissolved at 1 nM concentration in the different hydrogels were collected on a MicroTime 200 instrument (PicoQuant, GmbH), based on an Olympus IX-71 inverted confocal microscope. A 470 nm pulsed laser (PicoQuant LDH-P-C-470), controlled by a ''Sepia II'' driver, was used as the excitation source, working at a repetition rate of 20 MHz. The emitted fluorescence was collected through the 1.4 NA, $100\times$ oil immersion objective and focused onto a 75 μm pinhole, after passing through a 510dcxr dichroic mirror and a HP500LP cut-off filter (AHF/Chroma). After the pinhole, the fluorescence light was split into two channels by a 50/50 beam splitter, spectrally filtered by a 520/35 bandpass filter (Semrock) for channel 1 or a 550/40 bandpass filter (Thorlabs) for channel 2, and detected in two avalanche photodiode detectors (SPCM-AQR SPAD, Perkin-Elmer). The data acquisition was performed with a TimeHarp 200 time-correlated single photon counting (TCSPC) module, working in time-tagged time-resolved (TTTR) mode.[26] The incorporation of time-resolved fluorescence information within fluorescence correlation spectroscopy mea-surements has resulted in the so-called fluorescence lifetime

This journal is © The Royal Society of Chemistry and the Chinese Chemical Society 2018

Mater. Chem. Front., 2018, **2**, 686–699 | 689

correlation spectroscopy (FLCS), in which time-weighted filters are applied during the correlation to discriminate actual fluorescence photons from background noise or scattered light.[27] We performed FLCS cross-correlation (CC) between the two detection channels, as well as FLCS autocorrelation (AC) of the signal on the individual channels. The CC and ACF curves, $g(t)$, were fitted to the anomalous diffusion equation:

$$g(t) = g(0)\left[1 + \left(\frac{t}{\tau_D}\right)^{\alpha}\right]^{-1}\left[1 + \frac{1}{s^2}\left(\frac{t}{\tau_D}\right)^{\alpha}\right]^{-1/2} \quad (1)$$

where τ_D represents the diffusion time, $g(0)$ is the limiting amplitude, s is the geometrical parameter of the excitation volume (ratio between the vertical and the lateral focal radii), and α is the anomalous diffusion parameter. Subdiffusion effects appear when $\alpha < 1$. Apparent diffusion coefficients, D, were obtained as $s^2/4\tau_D$. In anomalous diffusion, the diffusion coefficients are time-dependent, hence, their values should only be taken as a qualitative approximation.[28] However, they can be useful to analyze the overall behavior and for detecting specific interactions between the dye and the gel fibers. The FLCS time filters, cross- and autocorrelations, and fittings were performed using the SymPhoTime 32 software (PicoQuant). During the fits, the geometrical parameter s was kept fixed as previously characterized.[29]

The fluorescence fluctuation traces of the dissolved dye were collected by focusing 10 μm inside the hydrogel. At least 15 traces of 150 seconds were obtained in different points of each hydrogel, containing different mass weights of FeNPs, with the gelification performed in the presence of a magnetic field as described above. Appropriate controls of the dye dissolved in the NMHG, and in MHG-0.1 and MHG-0.3 but gelified in the absence of the external magnetic field were also obtained.

Rheological characterization

We characterized the rheological properties of the NMHG and MHGs by using a Haake MARS III controlled-stress rheometer (Thermo Fisher Scientific, Waltham, MA, USA). The experimental characterization of the rheological properties of hydrogels presents special challenges due to some phenomena that are difficult to control, such as solvent loss,[30] changes in the microstructure caused by manipulation,[31] and even wall slip effects.[30,32] In order to avoid a wrong estimation of the rheological properties of our hydrogels due to the effect of these undesired phenomena, we used a double cone-plate geometry (60 mm in diameter and angle of 2°; sensor DC60/2° Ti L, Thermo Fisher Scientific, Waltham, MA, USA) for the characterization of the rheological properties, and we generated each of the hydrogels directly inside this geometry prior to measurement. For this method, we prepared the hydrogel-precursor mixture and immediately afterwards, we poured it in the cup of the measuring geometry, lowered down the double cone and covered with the upper plate. To avoid water evaporation, we created a supersaturated water atmosphere around the measuring geometry. Then, the mixture was left for gelation for 24 hours at 25 °C. For the application of a magnetic field during the initial steps of gelation, we used a coil placed coaxially with the axis of the double cone. After the 24 h period, we carried out the rheological characterization at 25 °C, without any prior preshear or manipulation, thus ensuring the unspoiled microstructure of the hydrogel. For each formulation we measured at least 3 different samples to ensure statistical significance of our results. We provide in this work the mean values and standard deviations of each magnitude. For a complete rheological characterization, we carried out different rheological tests, described in the following paragraphs.

Gelation kinetics. During the 24 hour gelation process, we monitored the evolution of the viscoelastic moduli (storage modulus, G', and loss modulus, G'') as a function of time, resulting from an oscillatory shear strain of amplitude 0.001 and frequency 1 Hz. Note that application of a low amplitude oscillatory shear is common practice to analyze sol–gel transitions – see, for example, the work by Winter.[33] The amplitude used in our work is up to one order of magnitude smaller than amplitudes used in previous studies for a similar purpose,[34] and should be low enough to ensure that the building of the gel microstructure was unperturbed. In fact, we verified that the rheological parameters of hydrogels not subjected to this oscillatory shear during gelation were not statistically different from those obtained for hydrogels subjected to it.

Rheological behavior under steady shear stress. After the 24 h gelation period was completed, we subjected the samples to ramps of step-wise increasing shear stress and the corresponding values of the shear strain were obtained. We maintained each value of shear stress for 10 s. The initial slope of the shear stress *vs.* shear strain is the rigidity modulus of the hydrogels.

Rheological behavior under oscillatory shear strain. After the 24 h gelation period was completed, we subjected the samples to oscillatory shear strain in order to characterize their viscoelastic response. First, we carried out ramps of oscillatory strains of fixed frequency (1 Hz) and increasing amplitude. Such measurements allow the identification of the linear viscoelastic region (LVR) as the low range of values of the strain amplitude for which the viscoelastic moduli (both G' and G'') are approximately independent of the magnitude of the strain amplitude. Above the LVR, G' decreases abruptly with the strain amplitude, whereas G'' usually increases first and then decreases. These changes in the values of G' and G'' mark the onset of the nonlinear viscoelastic region.[35] Once we delimited the LVR, we subjected the samples to ramps of constant shear strain amplitude (we chose the value 0.002, well within the LVR) and increasing frequency in the range 0–10 Hz. From these measurements, we obtained the trends of G' and G'' as a function of frequency, in the LVR.

Analysis of the mechanical anisotropy of the magnetic hydrogels. In order to analyze if the magnetic hydrogels gelled under a magnetic field presented anisotropic mechanical properties, we carried out additional rheological measurements using a parallel plate geometry. We used a parallel plate geometry (instead of a double cone-plate geometry) for these measurements since it was not possible to apply a magnetic field perpendicular to the axis of the rheometer due to set-up limitations. We proceeded as follows. We prepared the hydrogels (without FeNPs and containing

0.3 vol% of FeNPs) on disposable bottom plates (made of aluminum) of the rheometer, on which we previously carved a cylindrical hole of 2 mm depth and 35 mm diameter to avoid spreading of the content. The hydrogels were gelled for 24 hours under a water saturated atmosphere following the same protocol described above. In the case of magnetic hydrogels, we applied a magnetic field of 15 kA m^{-1} strength (with the help of a solenoid), either perpendicular (vertical) or parallel (horizontal) to the plane of the plate, during the first hour of gelation. After 24 hours, we placed the plate containing the hydrogel in the rheometer and descended the upper plate (35 mm in diameter; serrated surface to avoid wall slip) until perfect contact with the hydrogel was reached, without appreciable compression. Afterwards we carried out measurements under steady shear stress and under oscillatory shear strain, following the same protocols described above.

Results and discussion

Characterization of the magnetic particles

TEM micrographs revealed that FeNP powders were composed of spherical particles with a broad distribution in size (see Fig. S2 of the ESI†). Indeed, the particle size distribution of MNP fitted well to a Gaussian distribution (Fig. S3 of the ESI†), typical of particles resulting from growth starting from nuclei with negligible agglomeration.[36] The best fit to a Gaussian distribution function provided a mean diameter ± standard deviation of 73 ± 20 nm. TEM pictures also demonstrate the successful coating of MNP@PEG by a thin layer of PEG (Fig. S2 of the ESI†). Furthermore, the existence of a PEG layer around the particles was corroborated by measurements of the electrophoretic mobility of the nanoparticles (Fig. 2). As observed, the electrophoretic mobility significantly decreased for MNP@PEG with respect to PMNP for the whole range of pH values under study (from pH 4 to pH 11). Furthermore, the isoelectric point (zero mobility) for PMNP is close to the characteristic value of hematite (pH 7),[37] which is the iron oxide expected at the surface of iron. On the other hand, the isoelectric point of MNP@PEG is close to pH 4, considerably lower than that of PMNP. This is coherent with a PEG coating, since in this case, the surface of the nanoparticles is functionalized by hydroxyl groups and, thus, a trend to negative mobility is expected, as observed. Consequently, we can conclude that the particles were successfully coated by a PEG layer after treatment. In addition, the mobility was decreased even further after treatment with Fmoc-FF, which corroborates the adsorption of these molecules on MNP@PEG, also inferred from spectrophotometric measurements, as mentioned above. Note that for MNP@PEG@Fmoc-FF, measurements at pH 9 or smaller were impossible due to the formation of a gel. The treatment of MNP@PEG with Fmoc-FF peptide was carried out to improve the dispersion of the particles in the solution to originate homogeneous gels. In fact, when MNP@PEG particles were not pre-treated with Fmoc-FF, an inhomogeneous gel was obtained (data not shown). In this sense, all the experiments conducted in the hydrogels and discussed in the following
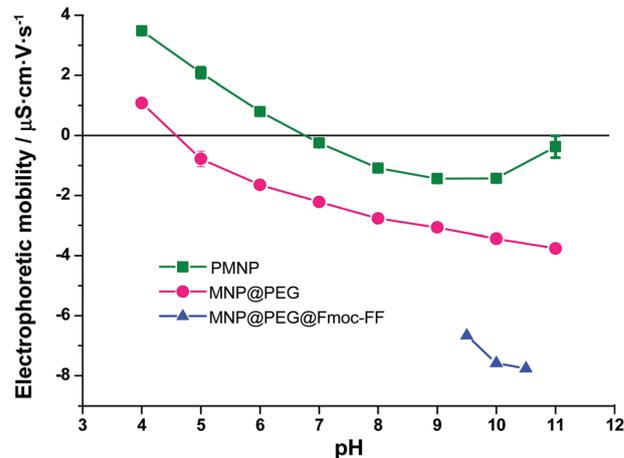

Fig. 2 Electrophoretic mobility of the nanoparticles.

subsections have been performed with these MNP@PEG@Fmoc-FF particles, for simplicity, sometimes mentioned as FeNPs.

Magnetization studies

The magnetization curve of the iron powders demonstrated a typical ferromagnetic behavior for both PMNP and MNP@PEG (Fig. S4 of the ESI†). From these curves, we obtained the values of the saturation magnetization (1521 ± 15 kA m^{-1} for PMNP and 1530 ± 12 kA m^{-1} for MNP@PEG) and the values of the remnant magnetization (62.3 ± 2.4 kA m^{-1} for PMNP and 75 ± 3 kA m^{-1} for MNP@PEG). From these data, as well as for the general shape of the magnetization curves (Fig. S4 of the ESI†), we may conclude that the coating by PEG has an almost negligible effect on the magnetic properties of the iron powder. Furthermore, in both cases, a rather soft ferromagnetic behavior is evidenced. The slightly higher values of saturation magnetization and remnant magnetization in the case of MNP@PEG with respect to PMNP can be attributed to protection against oxidation due to the coating with PEG – in the case of PMNP, a thicker layer of nonmagnetic oxide is expected at the surface.

Magnetization curves of magnetic hydrogels presented a similar shape to those of MNP@PEG, although with a much smaller saturation magnetization (Fig. 3). From these curves, we obtained the volume concentration of magnetic particles (ϕ) within the hydrogels using the mixing law of magnetism:[38] $M_{sh} = \phi \cdot M_s$, with M_{sh} and M_s being the saturation magnetizations of the hydrogels and MNP@PEG, respectively.

As observed, there is a good correspondence between concentrations according to preparation protocol and those obtained from magnetization measurements (Table S1 of the ESI†).

Morphology characterization

Optical microscopy studies. It is well known that the application of a magnetic field to a liquid-based suspension of magnetic particles induces the reversible formation of particle chain-like structures parallel to the direction of the applied field.[39] Brownian motion destroys such structures after field removal. Then, since we applied a magnetic field of 15 kA m^{-1}
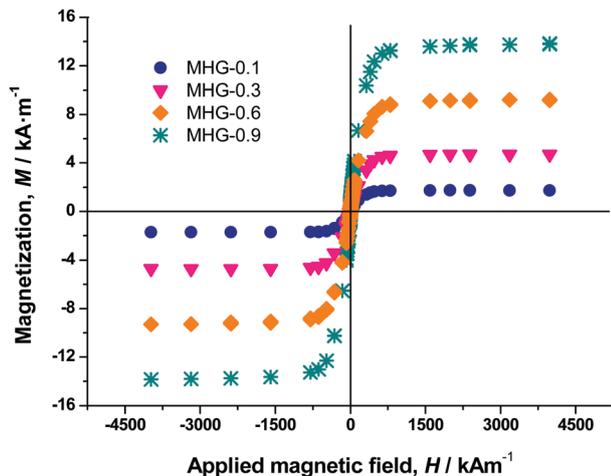
This journal is © The Royal Society of Chemistry and the Chinese Chemical Society 2018

Mater. Chem. Front., 2018, **2**, 686–699 | **691**

Fig. 3 Magnetization curves of magnetic hydrogels.

Fig. 5 ESEM of NMHG (A) and MHG-0.1 (B), MHG-0.3 (C) and MHG-0.6 (D).
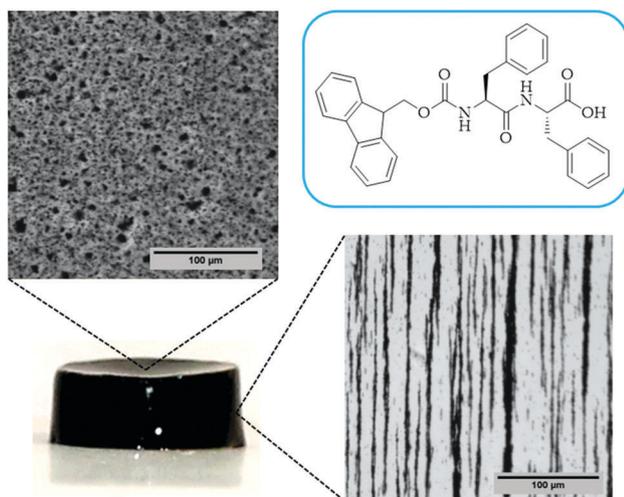

Fig. 4 Macroscopic picture of the hydrogel and optical images from the top and side views.

for 1 hour from the very beginning of the start of gelation, we expected that some FeNPs chains were built. Interestingly, as evidenced from optical microscopy (Fig. 4), some percolating column-like particle aggregates were observed to be homogeneously distributed throughout the final MHGs. This raises the question why the particle structures were maintained after field removal. The low remnant magnetization of the particles does not justify this observation and, consequently, the reason should be related to the interaction with the peptides, as we discuss in the next subsection.

Electron microscopy studies. Fmoc-FF peptide hydrogels have been studied before by electron microscopies.[40] It has been demonstrated that the gel-triggered conditions (solvent or pH switch) have a great impact on the final hydrogel microstructure. Additionally, the non-covalent nature of these aggregates made them very sensitive to external changes. For this reason, simple air-drying or more drastic procedures to obtain the xerogel can have an influence on the final morphology of the fibrils.
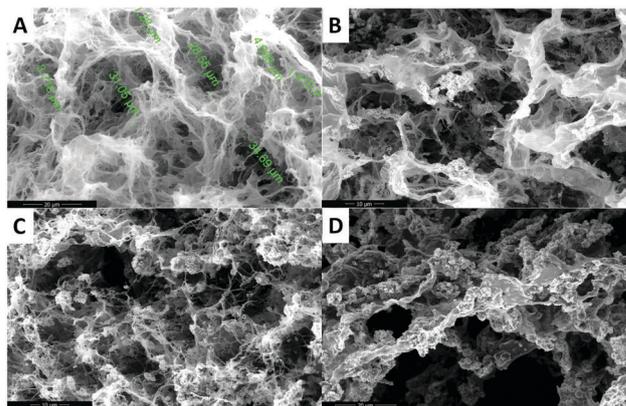
Although TEM and SEM images of xerogels have been successfully reported showing long nanofibers of 10 nm to 150 nm in diameter,[13] we decided to study the supramolecular arrangements of this peptide and peptide–FeNPs composites directly in the hydrogel medium. To accomplish this objective, we used an ESEM coupled with a Peltier to analyze the hydrogels under optimized temperature (-5 °C) and humidity (80%) conditions. As we can see in Fig. 5A, NMHG shows a dense network of branched ribbons and sheets, which differs significantly from the previously published reports based on xerogels. The tridimensional structure consists of a highly dense porous web with pores of different sizes.

In the case of the MHGs, we were interested to see whether the Fmoc-dipeptide would be able to maintain the same microstructural order or would be significantly challenged by the presence of the FeNPs considering that the gel is formed in the presence of them. Furthermore, we looked for some clue for the reason of the maintenance of the particle column-like structures (aggregates) after the field removal. As we can see in Fig. 5B–D, the supramolecular structure of the peptide is maintained in all samples to originate a macroporous web now decorated all over with FeNPs. A possible explanation may be that the FeNP aggregates are included in the structure simultaneously during fiber and sheet formation. Quite interestingly, the peptide supramolecular arrangement is able to withstand up to 0.6 vol% FeNP loadings without significantly altering its structure, which is quite impressive considering the small amount of the peptide involved in this process. At the same time, the different particles that constitute each of the column-like aggregates observed by optical microscopy seem to be fixed together by the peptide structure, which would justify the maintenance of the percolating particle aggregates after the magnetic field is switched off. Interestingly, this particular distribution of FeNP column-like structures within the peptide network drastically reinforces the gel matrix without practically altering the pore size, whilst, at the same time, it improves the diffusion of a solute through it, as will be seen below.

Secondary structure

Circular dichroism (CD) and Fourier transform infrared spectra (FTIR) were used to analyse and compare the secondary structure
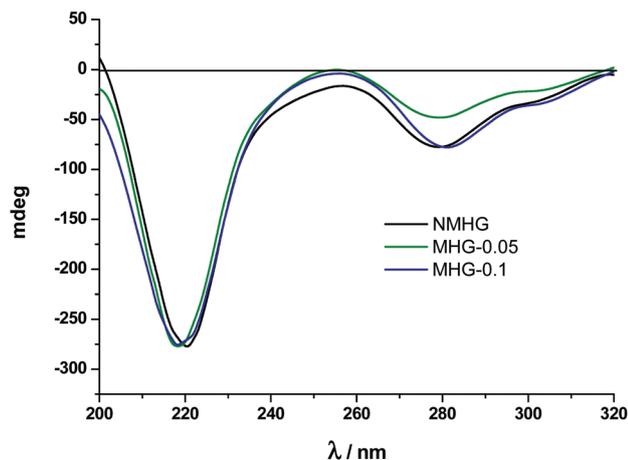
692 | Mater. Chem. Front., 2018, 2, 686–699

This journal is © The Royal Society of Chemistry and the Chinese Chemical Society 2018

Fig. 6 CD spectra of NMHG and MHG-0.05 and MHG-0.1.

Fig. 7 FTIR spectra of Fmoc-FF peptide, GdL, Fmoc-FF xerogel, NMHG and MHGs.

of NMHG and MHG to address the degree of degradability of the supramolecular arrangement of Fmoc-FF dipeptide. For this purpose, we carried out both studies in the gel phase. Although CD analysis of these hydrogels could be prone to artifacts and is very sensitive to gel concentration,[40a] we were mainly interested in the comparison between gels. It is also known that the spectra of the hydrogel are also very sensitive to experimental conditions used to prepare it.[41] In this sense, in our experimental conditions (pH switch using GdL), the CD spectrum of NMHG showed a maximum at 221 nm, which results from n–π transitions and at 279 nm, which corresponds to π–π transitions in the fluorenyl groups (Fig. 6).

Ulijn and coworkers have suggested that Fmoc-FF may be assembled in a β-sheet structure in the hydrogel prepared by pH switch using HCl.[40a] In our case, the n–π transition is slightly shifted to lower wavelength (from 218 nm to 222 nm). This can be due to the different concentrations used for both experiments (Ulijn et al.: 1.07 wt%) and this work (0.3 wt%). This phenomenon has already been described and can only mean that a higher peptide concentration indicates the presence of more β-sheet conformation.[42] Quite interestingly, the CD spectra of MHG-0.05 and MHG-0.1 showed a similar shape with the same two peaks at equal wavelengths (Fig. 6). These results indicate that the secondary structure derived from the self-assembly of the peptide practically remains unaltered in the presence of the FeNPs at these concentrations. Unfortunately, the CD spectra at higher FeNP concentrations could not be performed due to the light scattering caused by the sample.

To further corroborate these results, we performed FTIR spectroscopy on all hydrogels. The FTIR spectrum of the NMHG xerogel (Fig. 7, dark red line) showed two main peaks at 1651 and 1534 cm⁻¹. These bands can be assigned as the C=O stretching (amide I) and N–H bending (amide II) band, respectively.[42] With respect to the corresponding xerogel, the C=O stretching band (amide I) in the hydrogel NMHG (black line) is slightly red shifted (1645 cm⁻¹) and the band of the N–H bending (amide II) is slightly blue shifted (1536 cm⁻¹) indicating the formation of H-bonds.[42,43] Similar to previous reports,[40a,42]

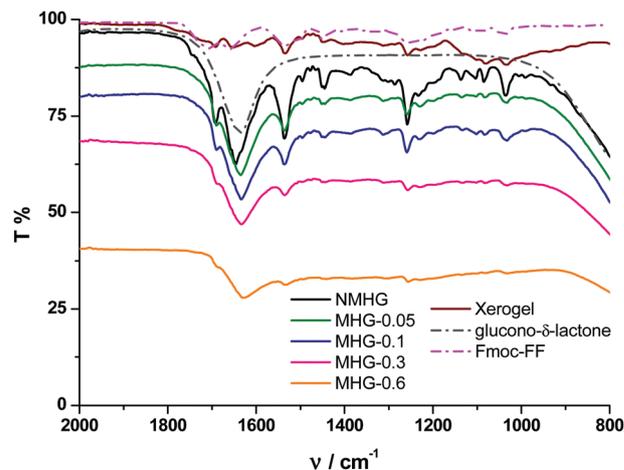the presence of two amide bands at 1645 and 1536 cm⁻¹ indicates a preference for a β-sheet conformation. Additionally, the presence of the band at 1692 cm⁻¹ suggests an antiparallel β-sheet arrangement for the self-association of the Fmoc peptide.[42] As we can observe from Fig. 7, the FTIR spectra of all MHGs have the same two amide bands at similar wavelengths to NMHG, which is in agreement with a β-sheet conformation and in line with the results observed in the CD. In this case, the amide I band in all the MHGs is red shifted to 1634 cm⁻¹. This shift may be due to an increase in the H-bond formation between the peptide and the PEG shell of the FeNPs. These results evidence that the dispersion and distribution of FeNP column-like structures within the gel matrix did not significantly alter the secondary structure of the peptide. This phenomenon may be due to the smaller sizes of the metallic nanoparticles and their columnar aggregates with respect to the higher aspect ratio of the peptide supramolecular network. Also, the rigid FeNP column-like aggregates located at fixed positions under the influence of an external magnetic field could also minimize the disruption of the peptide self-assembly and secondary structure.

The XRD pattern of NMHG (curve a (blue) of Fig. S5 of the ESI†) is in good agreement with that previously reported for Fmoc-FF gels.[40a,44] It shows a series of diffraction peaks appearing at d-spacing values equal to d/n (where 2 < n < 6). These periodic reflections are consistent with the presence of flat ribbons formed by the parallel stacking along their long axis of single fibrils.[40a] Plotting the n-order against the peak position (as scattering vector, $q = (2\pi/\lambda)\sin\theta$), one can obtain the width of the single fibrils from the slope (inset in Fig. S5 of the ESI†). From the best linear fitting, we obtained a width of 26.1 Å for a single fibril, which is in perfect agreement with the values reported for similar gels.[40a] The spacing between peptides within the β-sheet structures, which typically ranges between 4 and 5 Å depending on the peptide sequence,[40a] appears at a d-spacing of 4.8 Å.

Unfortunately, the corresponding signals of the supramolecular structure in MHG-0.3 (curve b (green line) of Fig. S5 of the ESI†)
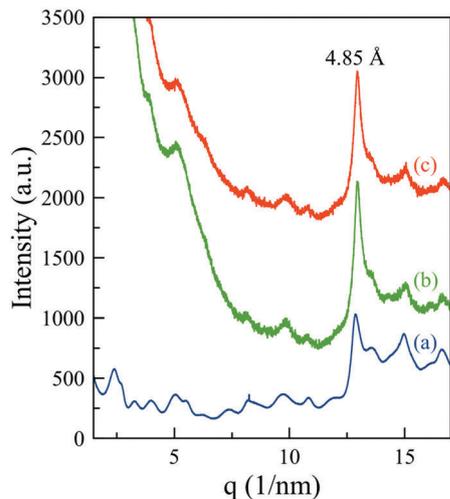
Fig. 8 Synchrotron X-ray total scattering patterns of NMHG (a) and MHG-0.3 in the absence (b) and presence (c) of magnetic fields.

are masked by the high scattering signal of the nanoparticles at such small angles (curve b of Fig. S5 of the ESI†). To solve this problem, we collected the synchrotron X-ray total scattering patterns of the naked and the particle-bearing gels at the X04SA materials science beam-line of the SLS-PSI (Fig. 8). The periodic reflections ($1 < n < 6$) were visible in the pattern of the NMHG (Fig. 8 – curve a, blue line), confirming the formation of ribbons of stacked 26 Å-width single fibrils. The spacing between peptides within the β-sheets also appeared at a *d*-spacing of 4.85 Å. All these features, although poorly defined due to the scattering of the nanoparticles in this angular region, were distinguishable in the patterns of MHG-0.3 prepared in the absence (Fig. 8 – curve b, green line) and presence (Fig. 8 – curve c, orange line) of a magnetic field. Hence, these results indicate that the supramolecular arrangement of the hydrogels is maintained even when they are prepared in the presence of an external magnetic field, in accordance with the CD and FTIR results.

FLCS studies

We were interested in knowing if the pore size distribution of the hydrogel network, and hence the diffusion of solutes through it, was significantly modified by the incorporation of the FeNPs. This is a fundamental question since traditional strategies that try to increase the mechanical properties of hydrogels imply a higher cross-linking, with the subsequent reduction in the pore size of the network hampering the diffusion of solutes through it. Alternative strategies, such as those described in the introduction do not guarantee an increase in the mechanical properties of the hydrogel or the maintenance of unaltered pore size or diffusion. This can be a serious drawback in certain biotechnological applications such as *in vivo* drug delivery and in tissue engineering where cells need adequate diffusion through the gel matrix for the interchange of nutrients and waste substances.

In this sense, the diffusion pattern of a small dye, **4-OMe-PG**, dissolved in the hydrogels was studied using FLCS. We chose this dye because of the low variation of the fluorescence
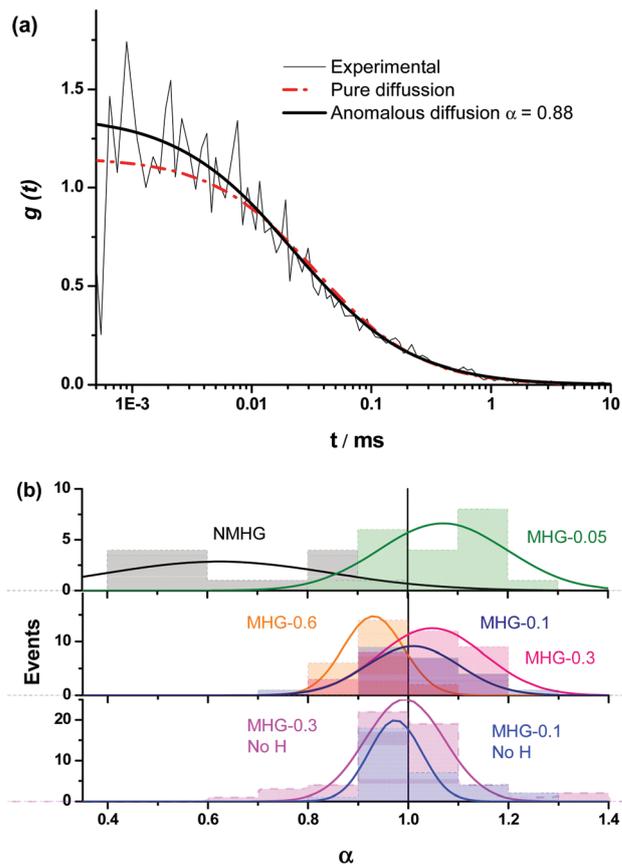

Fig. 9 (a) Representative FLCS-CC curve of **4-OMe-PG** dye in MHG-0.6, fitted to a pure diffusional model and to an anomalous diffusion equation. (b) Anomalous diffusion parameter α distributions for the **4-OMe-PG** dye in hydrogels without FeNPs (black), with 0.05 vol% (green), 0.1 vol% (royal blue), 0.3 vol% (pink), and 0.6 vol% (orange) FeNPs, formed with a magnetic field, and in hydrogels with 0.1 vol% (blue) and 0.3 vol% (magenta) FeNPs, formed in the absence of the magnetic field.

features of fluorinated xanthenes at near-neutral pH.[31,45] The AC and CC correlation curves of the dye in the MHGs showed a diffusional behavior very close to pure diffusion (Fig. 9a). Indeed, the α values ranged from 0.8 to 1.2 in the different measurements. Fig. 9b shows the α value distributions for the dye in gels carrying different loads of FeNPs. These distributions were fitted to a Gaussian function, in order to obtain the average value and the associated error (as the half-width of the function). The average α values were 1.07 ± 0.13, 1.01 ± 0.09, 1.05 ± 0.10, and 0.93 ± 0.06 for MHG-0.05, MHG-0.1, MHG-0.3 and MHG-0.6, respectively. A statistical comparison with $\alpha = 1$ showed that the samples with 0.05 vol%, 0.1 vol%, and 0.3 vol% of FeNPs were statistically not different from pure diffusional behavior (*p* value > 0.03). This implies that the **4-OMe-PG** dye diffuses similarly in the hydrogel to in bulk solvent. Furthermore, the obtained apparent diffusion coefficients were 380 ± 130, 450 ± 170, and 400 ± 110 μm^2 s^{-1}, for the dye in MHG-0.05, MHG-0.1 and MHG-0.3, respectively. These values are in perfect agreement with the diffusion coefficient obtained for the free **4-OMe-PG** dye in an aqueous solution of 410 ± 70 μm^2 s^{-1}, after fitting the FLCS-CC and AC functions to a pure diffusional model (with $\alpha = 1$).

Therefore, these values are in line with the diffusion coefficient of a small dye in aqueous solution, confirming the quasi-aqueous environment of the dye in the hydrogels. However, the population of samples in MHG-0.6 was statistically different from a pure diffusional behavior with a significance of 99% (p value = 3×10^{-6}). This means that the **4-OMe-PG** dye dissolved in the hydrogel with high loads of FeNPs presents a distinguishable subdiffusion behavior, although not very prominent. The average apparent diffusion coefficient for the dye in this gel was 540 ± 100 μm^2 s^{-1}. The apparent increase in the diffusion coefficient, compared to the other measurements, may be related to the formation of preferential channels for diffusion, restricting the pure 3D random walk of molecules. This effect is similar to the anomalous diffusion found for small dyes in the presence of large concentrations of crowding agents.[46] The excluded volume caused by the external agent makes the diffusion of the dye apparently faster compared to a freely diffusional environment. In any case, the effect is very mild, confirming that the aqueous nature of the hydrogel is mainly maintained, and that the pore size in these gels is larger than the size of the dye. As previously reported for agarose gels, when the diffusing dye is much smaller than the pore size of the gel, an α value around 0.93 described the shape of the autocorrelation functions[28] well and the dyes diffuse as if they were dissolved in homogeneous media. Although the refractive index mismatch between the probe medium and the glass may cause artifacts, such as the detection of an apparent anomalous diffusion behavior,[47] the detected curves are similar to a pure diffusional model, meaning that this effect is likely negligible.

In order to test whether the quasi-aqueous environment for the **4-OMe-PG** dye was promoted by the microscopic structure of the hydrogels being controlled by the long range sorting of the FeNP column-like aggregates due to the magnetic field, we probed the diffusional behavior of the dye in the MHG-0.1 and MHG-0.3 hydrogels, but formed without an external magnetic field, and in the NMHG. Fig. 9b shows the α value distributions of the **4-OMe-PG** dye in these cases. Interestingly, the α distributions were very similar to the samples formed with and without the magnetic field. The average α values, obtained from the fits to a Gaussian function, were 0.97 ± 0.11 and 0.99 ± 0.08 for MHG-0.1 and MHG-0.3 respectively, formed without a field. Likewise, the average apparent diffusion coefficient values of the dye in such gels were 440 ± 190 and 410 ± 150 μm^2 s^{-1} for MHG-0.1 and MHG-0.3, respectively. The α distributions for these hydrogels were not statistically different from $\alpha = 1$ (p values >0.4), confirming also the quasi-aqueous environment of the dye in the gels. The most striking result was obtained, however, with the NMHG. The diffusion of the **4-OMe-PG** dye in this gel was clearly anomalous, with an average $\alpha = 0.62 \pm 0.22$ (Fig. 9b), suggesting a more intricate micro-environment for the dye.

In conclusion, a small dye, such as **4-OMe-PG**, finds a quasi-aqueous environment in the gels formed with FeNPs and a magnetic field, caused by the formation of preferential channels for diffusion. The formation of hydrogels with FeNPs, but in the absence of a magnetic field, leads to a very similar micro-environment. This gel microstructure largely contrasts with that

of the hydrogel without FeNPs, which exhibits a diffusion in agreement with a close and tight network of fibrils. This difference in structures is in agreement with the information obtained in the ESEM images (Fig. 5).

Rheological studies

Gelation kinetics. As described above, we monitored the evolution of G' and G'' as a function of time in order to analyze the kinetics of gelation of our hydrogels. As observed, both G' and G'' increased strongly with time in the initial steps of the gelation process (up to approx. 200 s) – see results for MHG-0.05 as an example in Fig. S6 of the ESI.† Afterwards, the increase in moduli continued at a lower rate, although there was again a stronger increase around 20 000 s. Finally, the values of both G' and G'' leveled off for times larger than approximately 50 000 s (approx. 14 hours). Similar trends were obtained for other hydrogels (not shown). Comparison between gelation kinetics for different hydrogels evidenced a faster growth of G' and G'' with time for magnetic hydrogels with respect to nonmagnetic hydrogels, although there was not a clear tendency to a faster gelation kinetics by increasing the content of FeNPs. Furthermore, as observed in Fig. S6 of the ESI,† from the very beginning of the experiments G' was larger than G'' (characteristic of the presence of a gel-like material), which is an indication of the immediate crosslinking, as soon as the GdL was added. This is not surprising since the addition of the GdL causes the immediate formation of fiber-like structures that interact by overlapping.[24] Nevertheless, completion of the crosslinking process required very long times (more than 12 hours) as evidenced from the fact that the visco-elastic moduli continued to increase very quickly during this time.

Rheological behavior under steady shear stress. As observed, within the range of shear strains studied in our work, the shear stress shows an increasing linear trend with the shear strain for both NMHG and MHG (Fig. S7 of the ESI†). This linear dependence is characteristic of the linear region that viscoelastic materials present at low deformation. The effect of magnetic nanoparticles on the steady state rheological behavior of hydro-gels within the linear regime is best described by the slope of shear stress *vs.* shear strain curves. This slope is the shear (or rigidity) modulus, which is usually used as a measure of the strength of a material. As observed, the rigidity modulus of our hydrogels increased strongly with nanoparticle concentration up to 0.1 vol% (Fig. 10). Note that this tiny concentration of nanoparticles provoked a 4-fold increase in the value of the shear modulus with respect to the hydrogel without nanoparticles. Above this concentration and up to 0.6 vol%, the shear modulus still increased, although at a lower rate. However, a further increase in nanoparticle concentration did not provoke any additional enhancement of the shear modulus, but rather a tendency to decrease. Note that associated with the saturation of the mechanical enhancement at a high nanoparticle content (0.9 vol%), there was a lack of homogeneity and preparation became more difficult. Note also that when a magnetic field was not applied during gelation, we did not obtain any enhancement of the rigidity modulus (or other mechanical parameters) with respect to NMHG. Such a global trend, with an initial enhancement of

This journal is © The Royal Society of Chemistry and the Chinese Chemical Society 2018

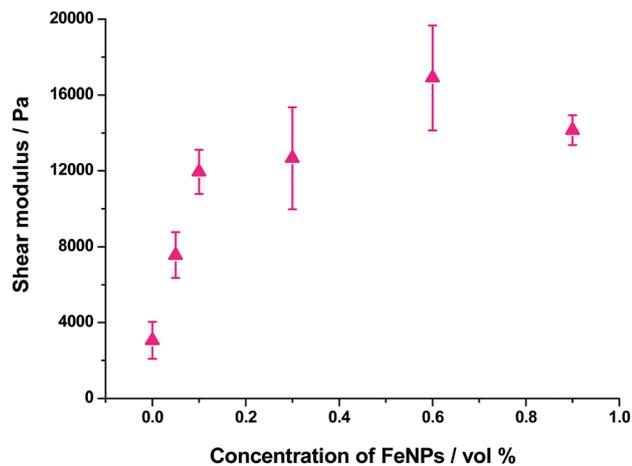*Mater. Chem. Front.,* 2018, **2**, 686–699 | **695**

Fig. 10 Variation of shear modulus with nanoparticle concentration.

mechanical strength of gels when nanoparticles are added at a low concentration, followed by a leveling off (or even decrease) of the mechanical strength at larger concentrations, has been previously reported in the case of polymeric gels.[48,49] Bonhome-Espinosa *et al.* found that the enhancement of the mechanical strength observed when nanoparticles were added was due to their role as knots for the crosslinking of the polymer fibers.[49] At larger concentrations of nanoparticles, the polymer network was so much disturbed by the presence of nanoparticles that the formation of a 3-D network of polymer chains started to fail, and thus their mechanical strength diminished.

In the case of the present work, a different hypothesis should be given since the secondary structure of the peptide hydrogel was practically unperturbed by the introduction of the particles. As discussed before, some column-like particle aggregates were induced by the magnetic field at the start of gelation. Then, during the peptide gel formation, the FeNPs were assimilated within the peptide structure, which was able to withstand the column-like aggregates, as evidenced by optical microscopy (Fig. 4). Our hypothesis is that these column-like particle aggregates served as some microscopic scaffold on which the secondary structure of the peptide gel was supported, giving a superior mechanical strength to the resulting hydrogels. From the optical microscopy, it is evident that the resulting particle structures are percolating. Furthermore, from the theoretical point of view, the following analysis can be made. In a first approximation, the particle structures induced by the field can be considered as long cylinders aligned in the direction of the applied field (unit vector e_1), whereas the applied shear stress is τ_{12}. Then, according to the most common model for the mechanical properties of composite materials with cylinder inclusions, introduced by Hashin and Rosen,[50] we have the following expression for the shear modulus of the composite in the cylinder direction, G_{12}:

$$G_{12} = G_m \frac{G_c(1 + \Phi) + G_m(1 - \Phi)}{G_c(1 - \Phi) + G_m(1 + \Phi)} \quad (2)$$

where G_m and G_c are respectively the shear modulus of the continuous matrix and the cylinders (nonmagnetic peptide hydrogel and elongated particle aggregates in the present work), and Φ is the volume fraction of the cylinders (that should be of the same order of magnitude as the volume fraction of the magnetic nanoparticles). However, from this expression, it is evident that even for completely rigid cylinders ($G_c \to \infty$), the enhancement in G_{12} with respect to G_m is almost negligible for Φ of the order of 0.01, as in the present work. However, if we have percolating structures, we may approximate the shear modulus of the composite in the cylinder direction by the theoretical prediction of the shear modulus of a mixture, which is given by:[18]

$$G_{12} = \Phi G_c + (1 - \Phi)G_m \quad (3)$$

This trend predicted by formula (3) fits perfectly with the experimental data for the shear modulus corresponding to volume fractions up to 0.001 (adj. R-square equal to 0.99991), with $G_c = 92100 \pm 600$ Pa and $G_m = 3060 \pm 40$ Pa. These data indicate that the shear modulus of the particle structures should be about 30 times stronger than the shear modulus of the peptide hydrogel, which seems reasonable taking into account that magnetic nanoparticles made of iron are inter-penetrated and interwoven by the self-assembled peptide. This composite material originates a structure similar to reinforced concrete, in which a skeleton of steel wires are filled with cement. Concerning the tendency of the shear modulus to level off at volume fractions higher than 0.001, the likely reason is the progressive difficulty of the peptides to give consistency to the particle structures and to hold them.

Rheological behavior under oscillatory shear strain. The trend of G' and G'' as a function of shear strain amplitude for oscillatory experiments at a fixed frequency of 1 Hz demonstrated a typical behavior of cross-linked systems – see as an example trend, MHG-0.05 in Fig. S8 of the ESI;† similar trends were obtained for other hydrogels. As observed, at low enough shear strain amplitude, both G' and G'' present an almost constant value. This region is identified as the linear viscoelastic regime (LVR). Within the LVR, G' is much larger (almost two orders of magnitude) than G''. In other words, the elastic response of the hydrogel (storage of energy) dominates over its viscous response (loss of energy), as expected for cross-linked systems. At larger values of the strain amplitude, G'' exhibits a rather noticeable enhancement, followed by a maximum for an approximate strain amplitude of 0.03. This maximum in G'' (maximum in loss of energy) corresponds to the yielding (irreversible destruction) of the hydrogel.[35] For even larger values of the strain amplitude, both G' and G'' decrease strongly and eventually they cross at large enough strain amplitude. Additionally, we performed oscillatory measurements of the hydrogels after extrusion using a syringe and confirmed that the hydrogels (both magnetic and non-magnetic) retained their gel-like nature, characterized by G' values higher than G'' within the LVR (Fig. S9 of the ESI†).

As mentioned above, all hydrogels (magnetic and non-magnetic) of the present work presented a similar trend of G' and G'' as a function of strain amplitude. The main difference was the relative values of these magnitudes that increased strongly with FeNP concentrations up to 0.1 vol%, and then

696 | *Mater. Chem. Front.,* 2018, **2**, 686–699

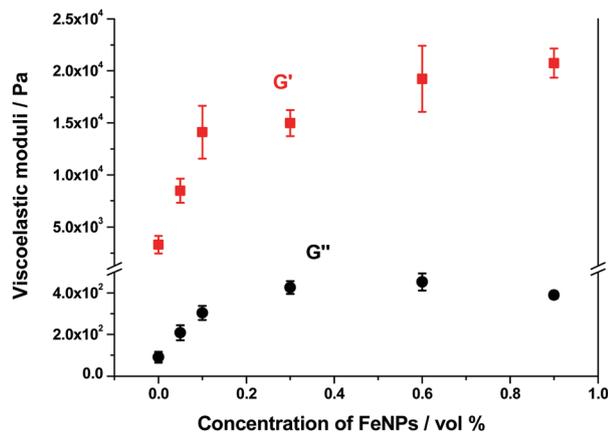This journal is © The Royal Society of Chemistry and the Chinese Chemical Society 2018

Fig. 11 Representation of viscoelastic moduli against concentration of FeNPs.

at a smaller rate with a tendency to level off at concentrations above 0.6 vol% – see a plot with the values corresponding to the LVR in Fig. 11. Note that an increase of G' of approx. 7 times is obtained for the highest concentration of FeNPs (0.9 vol%) with respect to the NMHG. This trend is similar to the one discussed above for the shear modulus.

Other parameters that depend on FeNP concentration are the amplitudes of the shear strain and the shear stress corresponding to the yield point (peak value of G'' in curves like this of Fig. S8 of the ESI†). In the case of these hydrogels, the shear strain at the yield point showed a tendency to decrease as the content of FeNPs increased, whereas the shear stress at the yield point increased with FeNP content (Fig. S10 of the ESI†). We obtained similar trends (not shown here) for the critical shear strain and critical shear stress that marked the onset of the nonlinear viscoelastic region. In overall terms, we can conclude that as FeNPs are included at a larger proportion in the composition of these supramolecular hydrogels (prepared under an applied magnetic field), the resulting magnetic hydrogels become tougher and, accordingly, their strain at fracture diminishes.

Finally, we also obtained the oscillograms (curves of G' and G'' as a function of frequency of oscillatory shear strain) corresponding to the LVR (Fig. 12). As observed, trends are similar for NMHG and MHGs, independent of the concentration of magnetic nanoparticles, where the values of G' and G'' are the only distinctive difference between the curves corresponding to different hydrogels. In all cases, G' showed a constant value within the whole range of frequencies under study. As for G'', first it increased smoothly with frequency, then it reached a maximum around a frequency of 4 Hz, afterwards it decreased sharply, and finally showed a tendency to level off at the highest frequencies. The independence of G' on the frequency of the oscillatory shear, as well as the smooth increase of G'' with frequency, are typical of strongly cross-linked systems, like rubber.[51] Concerning the decrease of G'' observed around 4 Hz, it has been previously observed for polymer hydrogels.[49]

Analysis of the mechanical anisotropy of the magnetic hydrogels. These magnetic hydrogels present a clear anisotropic
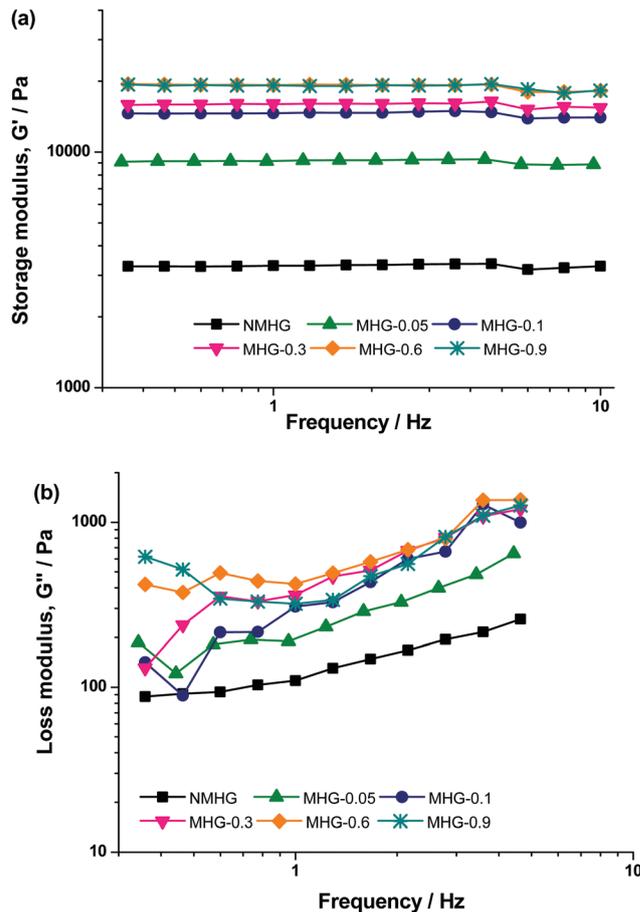

Fig. 12 Oscillograms corresponding to the LVR of NMHG and MHGs: (a) storage modulus *vs.* frequency and (b) loss modulus *vs.* frequency.

Table 1 Data of storage and loss moduli for MHG-0.3 prepared under horizontal (MHG-0.3H) or vertical (MHG-0.3V) magnetic fields, with respect to the plane of the disk-like hydrogel and the plane of shear. For comparison, data for NMHG are also included. Similar trends were obtained for the shear modulus, not shown here for brevity

Hydrogel	Storage modulus (Pa)	Loss modulus (Pa)
NMHG	2960 ± 160	209 ± 8
MHG-0.3H	1120 ± 120	124 ± 13
MHG-0.3V	5900 ± 300	352 ± 23

behavior, evidenced by smaller rheological moduli than that of NMHG when the shear was applied in the same plane as the magnetic field, and higher rheological moduli when the shear was applied perpendicular to the direction of the magnetic field (Table 1). This anisotropy highlights the strong influence that the FeNP column-like aggregates have on the final macroscopic mechanical properties of the hydrogels.

Conclusions

Novel short-peptide supramolecular magnetic hydrogels have been prepared by the self-assembly of Fmoc-FF in a suspension containing iron nanoparticles (FeNPs) in the presence or

absence of an external magnetic field. The influence of the magnetic field modifies the structural characteristics of the hydrogels inducing the formation of FeNP column-like aggregates. The resulting anisotropic structure composed of vertically aligned FeNP columns-like aggregates engulfed by the peptide fibers is responsible for the enhancement in the mechanical properties of these hydrogels. As far as we know, this is the first time that such an enhancement in the mechanical properties of a supramolecular hydrogel has been mediated by the presence of FeNPs, and can only be explained due to the particular characteristics of this material, in which the non-covalent nature of the peptide self-assembly is essential. Quite interestingly, the peptide β-sheet secondary structure is conserved as well as the pore size, making this one of the few examples in which the mechanical strength of the gel is enhanced without significantly altering the microstructure of the gel network and improving the diffusion of a solute through it.

Conflicts of interest

There are no conflicts of interest to declare.

Acknowledgements

References

1 (a) M. Ebara, et al., Smart Biomaterials, NIMS Monographs, National Institute for Materials Science, Japan, Springer Japan, 2014, DOI: 10.1007/978-4-431-54400-5; (b) A. Döring, W. Birnbaum and D. Kuckling, Chem. Soc. Rev., 2013, 42, 7391.

2 (a) E. I. Anastasova, V. Ivanovski, A. F. Fakhardo, A. I. Lepeshkin, S. Omar, A. S. Drozdov and V. V. Vinogradov, Soft Matter, 2017, 13, 8651; (b) A. Campanella, O. Holderer, K. Raftopoulos, C. Papadakis, M. Staropoli, M. Appavou, P. Müller-Buschbaum and H. Frielinghaus, Nanotechnology (IEEE-NANO), 2016 IEEE 16th International Conference on, 2016, p. 446; (c) J. Thévenot, H. Oliveira, O. Sandre and S. Lecommandoux, Chem. Soc. Rev., 2013, 42, 7099.

3 (a) Y. Li, G. Huang, X. Zhang, B. Li, Y. Chen, T. Lu, T. J. Lu and F. Xu, Adv. Funct. Mater., 2013, 23, 660; (b) J. Zhang, S. Xu and E. Kumacheva, J. Am. Chem. Soc., 2004, 126, 7908.

4 (a) C. D. Jones and J. W. Steed, Chem. Soc. Rev., 2016, 45, 6546; (b) X. Du, J. Zhou, J. Shi and B. Xu, Chem. Rev., 2015, 115, 13165–13307.

5 A. Wang, W. Shi, J. Huang and Y. Yan, Soft Matter, 2016, 12, 337.

6 (a) K. Tao, A. Levin, L. Adler-Abramovich and E. Gazit, Chem. Soc. Rev., 2016, 45, 3935; (b) S. Fleming and R. V. Ulijn, Chem. Soc. Rev., 2014, 43, 8150; (c) A. Dasgupta, J. H. Mondal and D. Das, RSC Adv., 2013, 3, 9117.

7 E. R. Draper and D. J. Adams, Chem, 2017, 3, 390.

8 (a) D. J. Cornwell and D. K. Smith, Mater. Horiz., 2015, 2, 279; (b) M. Conejero-Muriel, R. Contreras-Montoya, J. J. Díaz-Mochón, L. Álvarez de Cienfuegos and J. A. Gavira, CrystEngComm, 2015, 17, 8072; (c) M. Conejero-Muriel, J. A. Gavira, E. Pineda-Molina, A. Belsom, M. Bradley, M. Moral, J.-D. García-López Durán, A. Luque González, J. J. Díaz-Mochón, R. Contreras-Montoya, Á. Martínez-Peragón, J. M. Cuerva and L. Álvarez de Cienfuegos, Chem. Commun., 2015, 51, 3862.

9 (a) J. Raeburn, C. Mendoza-Cuenca, B. N. Cattoz, M. A. Little, A. E. Terry, A. Z. Cardoso, P. C. Griffiths and D. J. Adams, Soft Matter, 2015, 11, 927; (b) J. Raeburn, G. Pont, L. Chen, Y. Cesbron, R. Levy and D. J. Adams, Soft Matter, 2012, 8, 1168; (c) L. Chen, J. Raeburn, S. Sutton, D. G. Spiller, J. Williams, J. S. Sharp, P. C. Griffiths, R. K. Heenan, S. M. King, A. Paul, S. Furzeland, D. Atkins and D. J. Adams, Soft Matter, 2011, 7, 9721; (d) W. Helen, P. D. Leonardis, R. V. Ulijn, J. Gough and N. Tirelli, Soft Matter, 2011, 7, 1732.

10 (a) V. Jayawarna, S. M. Richardson, A. R. Hirst, N. W. Hodson, A. Saiani, J. E. Gough and R. V. Ulijn, Acta Biomater., 2009, 5, 934; (b) M. Zhou, A. M. Smith, A. K. Das, N. W. Hodson, R. F. Collins, R. V. Ulijn and J. E. Gough, Biomaterials, 2009, 30, 2523.

11 (a) G. Pont, L. Chen, D. G. Spiller and D. J. Adams, Soft Matter, 2012, 8, 7797; (b) L. Chen, S. Revel, K. Morris, D. G. Spiller, L. C. Serpell and D. J. Adams, Chem. Commun., 2010, 46, 6738.

12 J. Wang, Z. Wang, J. Gao, L. Wang, Z. Yang, D. Kong and Z. Yang, J. Mater. Chem., 2009, 19, 7892.

13 R. Huang, W. Qi, L. Feng, R. Su and Z. He, Soft Matter, 2011, 7, 6222.

14 J. Nanda, B. Adhikari, S. Basak and A. Banerjee, J. Phys. Chem. B, 2012, 116, 12235.

15 S. Roy and A. Banerjee, RSC Adv., 2012, 2, 2105.

16 B. Adhikari and A. Banerjee, Soft Matter, 2011, 7, 9259.

17 M. Ikeda, S. Ueno, S. Matsumoto, Y. Shimizu, H. Komatsu, K.-I. Kusumoto and I. Hamachi, Chem. – Eur. J., 2008, 14, 10808.

18 R. M. Christensen, Mechanics of Composite Materials, Krieger Publishing Company, Malabar, 1991.

19 M. C. Nolan, A. M. Fuentes Caparrós, B. Dietrich, M. Barrow, E. R. Cross, M. Bleuel, S. M. King and D. J. Adams, Soft Matter, 2017, 13, 8426.

20 Z. Yang, H. Gu, J. Du, J. Gao, B. Zhang, X. Zhang and B. Xu, Tetrahedron, 2007, 63, 7349.

21 L. Rodriguez-Arco, I. A. Rodriguez, V. Carriel, A. B. Bonhome-Espinosa, F. Campos, P. Kuzhir, J. D. G. Duran and M. T. Lopez-Lopez, Nanoscale, 2016, 8, 8138.

22 (a) R. Petros and J. M. De Simone, Nat. Rev. Drug Discovery, 2010, 9, 615; (b) M. Arruebo, M. Galan, N. Navascues, C. Tellez, C. Marquina, M. R. Ibarra and J. Santamaria,

Chem. Mater., 2006, **18**, 1911; (*c*) H. Otsuka, Y. Nagasaki and K. Kataoka, *Adv. Drug Delivery Rev.*, 2012, **64**, 246.

23 J. Chatterjee, M. Bettge, Y. Haik and C. J. Chen, *J. Magn. Magn. Mater.*, 2005, **293**, 303.

24 D. J. Adams, L. M. Mullen, M. Berta, L. Chena and W. J. Frith, *Soft Matter*, 2010, **6**, 1971.

25 V. Puente-Muñoz, J. M. Paredes, S. Resa, A. M. Ortuño, E. M. Talavera, D. Miguel, J. M. Cuerva and L. Crovetto, *Sens. Actuators, B*, 2017, **250**, 623.

26 M. Wahl, R. Erdmann, K. Lauritsen and H. J. Rahn, *Proc. SPIE*, 1998, **173**, 3259.

27 (*a*) S. Rüttinger, P. Kapusta, M. Patting, M. Wahl and R. Macdonald, *J. Fluoresc.*, 2010, **20**, 105; (*b*) P. Kapusta, M. Wahl, A. Benda, M. Hof and J. Enderlein, *J. Fluoresc.*, 2007, **17**, 43.

28 N. Fatin-Rouge, K. Starchev and J. Buffle, *Biophys. J.*, 2004, **86**, 2710.

29 J. M. Paredes, S. Casares, M. J. Ruedas-Rama, E. Fernández, F. Castello, L. Varela-Álvarez and A. Orte, *Int. J. Mol. Sci.*, 2012, **13**, 9400.

30 J. M. Piau, *J. Non-Newtonian Fluid Mech.*, 2007, **144**, 1.

31 D. Bonn and M. M. Denn, *Science*, 2009, **324**, 1401.

32 S. Aktas, D. M. Kalyon, B. M. Marin-Santibanez and J. Perez-Gonzalez, *J. Rheol.*, 2014, **58**, 513.

33 H. H. Winter, *Polym. Eng. Sci.*, 1987, **27**, 1698.

34 J. Cho, M. C. Heuzey and M. L. Hamdine, *Macromol. Mater. Eng.*, 2007, **292**, 571.

35 E. Moghimi, A. R. Jacob, N. Koumakis and G. Petekidis, *Soft Matter*, 2017, **13**, 2371.

36 K. Kimura, *Fine particles*, Marcel Dekker, Inc., 2000, pp. 513–551.

37 K. Quast, *International Journal of Mining Engineering and Mineral Processing*, 2012, **1**, 73–83.

38 R. E. Rosensweig, *Ferrohydrodynamics*, Cambridge University Press, Cambridge, 1985.

39 G. Bossis, O. Volkova, S. Lacis and A. Meunier, *Lect. Notes Phys.*, 2002, **594**, 201.

40 (*a*) A. M. Smith, R. J. Williams, C. Tang, P. Coppo, R. F. Collins, M. L. Turner, A. Saiani and R. V. Ulijn, *Adv. Mater.*, 2008, **20**, 37; (*b*) A. Mahler, M. Reches, M. Rechter, S. Cohen and E. Gazit, *Adv. Mater.*, 2006, **18**, 1365.

41 B. Ding, Y. Li, M. Qin, Y. Ding, Y. Cao and W. Wang, *Soft Matter*, 2013, **9**, 4672.

42 B. Adhikari, G. Palui and A. Banerjee, *Soft Matter*, 2009, **5**, 3452.

43 A. Banerjee, G. Palui and A. Banerjee, *Soft Matter*, 2008, **4**, 1430.

44 X. Mu, K. M. Eckes, M. M. Nguyen, L. J. Suggs and P. Ren, *Biomacromolecules*, 2012, **13**, 3562.

45 (*a*) L. F. Mottram, S. Boonyarattanakalin, R. E. Kovel and B. R. Peterson, *Org. Lett.*, 2006, **8**, 581; (*b*) A. Orte, L. Crovetto, E. M. Talavera, N. Boens and J. M. Alvarez-Pez, *J. Phys. Chem. A*, 2005, **109**, 734.

46 (*a*) S. Smith, C. Cianci and R. Grima, *J. R. Soc., Interface*, 2017, **14**, 0047; (*b*) H. Sanabria, Y. Kubota and M. N. Waxham, *Biophys. J.*, 2007, **92**, 313.

47 S. Lehmann, S. Seiffert and W. Richtering, *Macromol. Chem. Phys.*, 2015, **216**, 156.

48 D. Borin, D. Günther, C. Hintze, G. Heinrich and S. Odenbach, *J. Magn. Magn. Mater.*, 2012, **324**, 3452.

49 A. B. Bonhome-Espinosa, F. Campos, I. A. Rodriguez, V. Carriel, J. A. Marins, A. Zubarev, J. D. G. Duran and M. T. Lopez-Lopez, *Soft Matter*, 2017, **13**, 2928.

50 Z. Hashin and B. W. Rosen, *J. Appl. Mech.*, 1964, **31**, 223.

51 C. W. Macosko, *Rheology: principles, measurements and applications*, Wiley-VCH, Weinheim, 1994.

This journal is © The Royal Society of Chemistry and the Chinese Chemical Society 2018

Mater. Chem. Front., 2018, **2**, 686–699 | **699**